CO2 exchange in a temperate marginal sea of the Mediterranean Sea: processes and carbon budget

G. Cossarini, S. Querin, C. Solidoro

This file contains: the new section 3.2, the Appendix A and the Appendix B.

3.2 Modelled ecosystem dynamics

The validation of the model simulation, reported in Appendix B, has been performed using several different datasets (monthly satellite chlorophyll-a data, three seasonal climatological datasets of nutrient, oxygen and chlorophyll-a, and observations and estimates from literature for relevant ecosystem processes). The comparison proves that the model reproduces satisfactorly the main spatial gradients and trends of chlorophyll-a, and the seasonal and vertical variabilities of nutrients (DIP and DOP). Further, simulated values of relevant processes (primary production, sinking, burial, bacterial carbon production), which can have an influence on the consumption and production of organic carbon, and therefore on the carbon continental shelf pump, are consistent with literature data.

Different biological processes contribute to the carbon pump in the Adriatic Sea in different ways: the excess of primary production over respiration triggered by the river input in the western part of the NA and the phytoplanktonic blooms in the central part of the SA during winter deep convection events favour an adsorption of atmospheric CO_2. Moreover, during the summer stratification in the SA, the prevalence of respiration on primary production supports the accumulation of dissolved inorganic carbon in the water column.

In the NA, modelled freshwater input from rivers (the Po River and other rivers) generates a current that flows southwards along the Italian coast (the Western Adriatic Current, WAC, Querin et al., 2012). Within the WAC, the simulated DIP concentrations are high, due to the river discharges, whereas the DIP levels offshore are low (Fig. B5 and Tab. B2 in Appendix B). The seasonal cycle shows higher DIP concentrations in autumn and winter when simulated mineralization prevails over uptake, and external inputs are higher. In contrast, lower DIP concentrations are simulated during spring and summer when biological uptake prevails (Table B2 in Appendix B). For the central (CA) and southern (SA) basin, the model reproduces oligotrophic conditions (a DIP concentration less

than 0.05 mmol/m^3) for the surface layer, whereas the deep layers of the CA and SA are characterised by DIP accumulation (concentrations greater than 0.1-0.15 mmol/m^3, Fig. 6, Table B2).

As a consequence of the nutrient availability, the model produces a chlorophyll-a rich strip along the Italian coast (sequence of maps in Fig. B1), which is a permanent feature that has been observed in the MODIS (Volpe et al., 2012) and SeaWifs (Barale et al., 2005) satellite images. The simulated chlorophyll-a concentrations and dynamics are consistent with the observed values (Fig. B1 and B2 in Appendix B). The productivity of this eutrophic coastal strip is significantly higher than the off-shore productivity (Fig. 4 and Tab. B4). Therefore, the western part of the NA is a prominent zone for the biological carbon pump, in fact, the excess of the production over community respiration during winter-spring (Fig. 4) causes a net production of organic matter which is advected southwards and out of the northern continental shelf. When plankton production and dense water formation occur at the same time (next sections), organic matter sinks and spreads in the deeper layers of CA and SA.
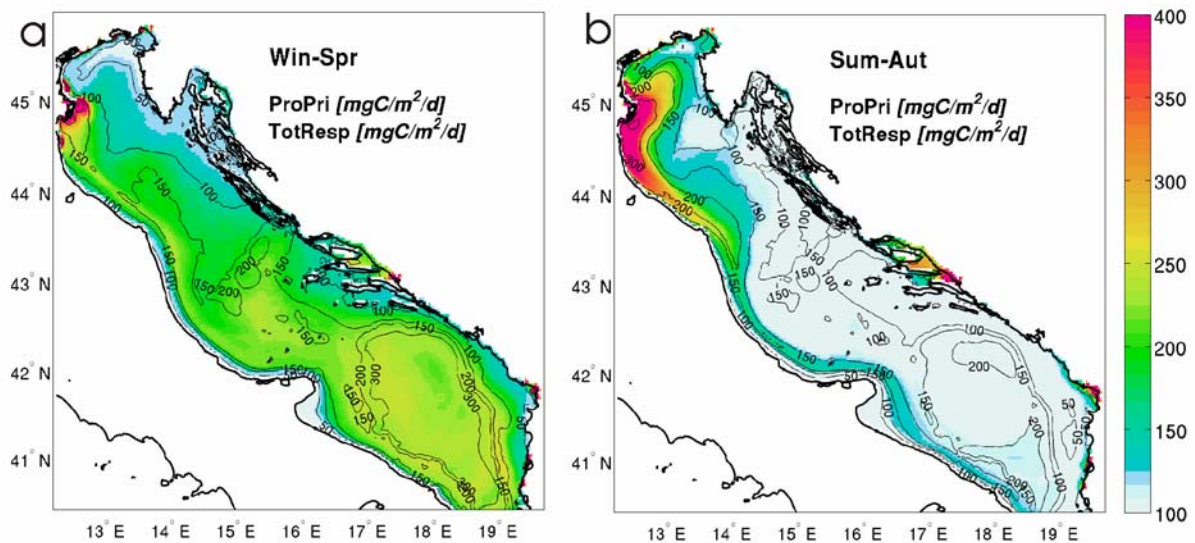
Fig. 4. Simulated mean bi-seasonal primary production (colours) and community respiration (contour lines) integrated over the water column.

The SA is oligotrophic, with low levels of chlorophyll-a and productivity (Fig. B1 and Fig. 4). The contribution of the eutrophic WAC is weak and restricted to a narrow strip along the Italian coast, whereas the input from the Neretva River and other south-eastern rivers trigger important local

chlorophyll-a signals in the eastern Adriatic Sea (Fig. B1 and Fig. 4), as observed by Marini et al. (2010).

The open ocean convection, driven by negative heat fluxes (Gačić et al., 2002) during winter, breaks off the oligotrophic condition of the SA, causing a significant increase in productivity (Fig. 4). The convection causes deep mixing and nutrient upwelling which sustain a phytoplankton bloom in the centre of the pit (Santoleri et al., 2003; Batistić et al., 2011) according to the Gran effect two-phase process (see Mann and Lazier, 1998). Model results (Fig. 5) show that during the first phase of intense vertical mixing, phytoplankton productivity is limited by the downward transport of phytoplankton biomass, and significant phytoplankton concentrations are simulated even at depths below the photic zone, as observed during samplings in February 2010 (Batistić et al., 2011). After this first phase, the upward flux of nutrients and the occurrence of thermal stratification trigger a surface bloom that has also been detected in satellite maps (Santoleri et al., 2003). The modelled blooms are dominated by diatoms (not shown): this is consistent with the experimental observations of Boldrin et al. (2002). As the summer stratification develops, a deep chlorophyll-a maximum is reproduced by the model at depths of approximately 50 m (Fig. 5): this is also consistent with observational data (Boldrin et al., 2002).

During summer, the SA shows the prevalence of respiration processes (Fig. 4), which consumes the sunk organic matter produced during the winter bloom or advected from the NA by the WAC and by the dense water spreading.
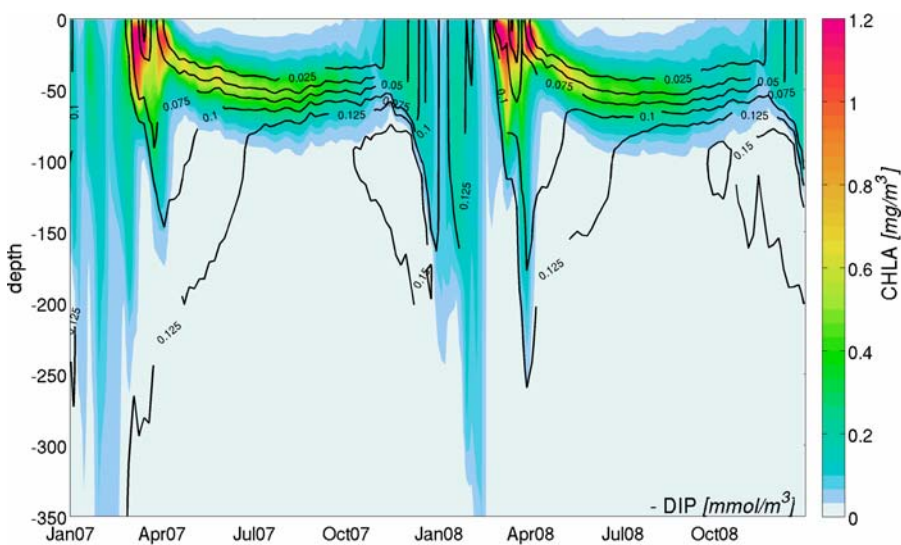
Figure 5. Hovmöller diagram of chlorophyll-a (shaded plot) and DIP (contour plot) in a station located in the southern Adriatic pit (see the location (star symbol) in Fig. 1).

CO2 exchange in a temperate marginal sea of the Mediterranean Sea: processes and carbon budget
G. Cossarini, S. Querin, C. Solidoro

Appendix A: Model formulation

The biogeochemical model describes the variation of the 13 state variables shown in Figure 2. The rate of change of each state variables is defined by

$$\frac{\partial C}{\partial t} = -U \cdot \nabla C + \nabla_H K_h \nabla_H C + \frac{\partial}{\partial z}\left[K_v \frac{\partial C}{\partial z}\right] + w_s \frac{\partial C}{\partial z} + \frac{\partial C}{\partial t}\Big|_{bio}$$

where the first four terms describe the variation due to transport processes (advection, horizontal and vertical diffusion and sinking) and the fifth term describes the variation due to chemical reactions and biological relationships among the functional groups. The transport equations are resolved by internal packages (*ptracer* and *gchem*) of the MITgcm code (Adcroft et al., 2011), where velocity and diffusivity fields are computed by the core of the physical part of the MITgcm model (Marshal et al., 1997). A customization of the MITgcm model has been properly developed for the Adriatic Sea (Querin et al., 2012). The biogeochemical model has been coded as subroutine within the package *ptracter* of the MITgcm code. The coupling of the transport and biogeochemical models uses an "operator splitting" method, with an integration time of 300 s for both physical and biogeochemical models. Even if operator splitting schemes are suggested to be less accurate than source splitting schemes (Butenschön et al., 2012), the use of a very short integration time makes the model output less sensitive to the choice of the scheme.

The biogeochemical model simulates the carbon and phosphorus cycles (Fig. 1), and it is developed to reproduce two trophic and energy path ways: the classic food chain and the microbial food web (Cushing, 1989; Legendre and Rassoulzadegan, 1995). Diatom *[Phy2]* and mesozooplankton *[Zoo2]* groups are the compartments involved in the classic food chain, which comprises groups with the highest primary and secondary production rates and drives carbon flows mainly towards particulate organic carbon *[POC]* and export production. Under more oligotrophic conditions, the microbial food web prevails, where the interaction between small phytoplankton *[Phy1]*, small zooplankton *[Zoo1]* and bacteria *[Bac]* is sustained via the rapid recycling of nutrients, and the carbon cycle primarily involves dissolved organic carbon *[DOC]*. As regard the *[DOC]*, the model simulates only its labile part, which represents around 10-30% of the DOC concentration in the study area (Cossarini et al., 2012). Carbon and phosphorus dynamics in the particulate and dissolved organic compartments are uncoupled.

The biogeochemical model is resulting from an upgrade of the original version (Cossarini and Solidoro, 2008) through the inclusion of the carbonate system, which required the simulation of two new state variables: dissolved inorganic carbon *[DIC]* and alkalinity *[ALK]*. The rate of change of alkalinity accounts for the uptake of nutrient ions by biological cells. Since the solely nutrient in the model is phosphorus, its rate of change is multiplied by a coefficient that accounts for the contribution of the all nutrients (Wolf-Gladrow et al., 2007). The rate of variation of DIC is computed as function of the production and consumption terms of the phytoplankton and bacteria functional groups (Lazzari et al., 2012). The carbonate system is solved by the standard OCMIP II model (Orr et al., 1999), whereas the air-sea exchange of CO_2, which impacts the DIC at the surface layer, is computed using the parameterisation by Follows et al. (2006). Bacterial lysis has been modified from Cossarini and Solidoro (2008) by adding an oxygen dependent parameterization (Lazzari et al., 2012). The dependence of alkaline phosphatase on the phosphorus availability (Hoppe, 2003; Labry et al., 2005) has been added in order to enhance remineralization rate in oligotrophic conditions, like those of the southern Adriatic Sea. The sinking is active only for phytoplankton groups and particulate organic matter: the latter reaches the bottom layer, accumulates in the upper sediment, and it is remineralized and partly buried. Sediment remineralization, which produces DOP and DOC, is described by a first order kinetic of the sunk particulate organic material. The dissolved organic pools are then consumed and respired by bacteria releasing DIP and DIC. The biogeochemical state variables are listed in Tab. A1. The rate of change for biogeochemical state variables is defined in Tab. A2, whereas the parametrizations and their kinetic constants are reported in Tab. A3 and A4 respectively.

symbols	names in Fig. 2	State variables	Unit
[Phy1]	Nphy	small phytoplankton	mmolC/m^3
[Phy2]	diatom	diatom	mmolC/m^3
[Zoo1]	µzoo	microzooplankton and heterotrophic nanoflagellates	mmolC/m^3
[Zoo2]	Mzoo	mesozooplankton -	mmolC/m^3
[Bac]	bac	heterotrophic picoplankton	mmolC/m^3
[DIC]	DIC	dissolved inorganic carbon	mmolC/m^3
[DOC]	DOC	dissolved organic carbon	mmolC/m^3
[POC]	POC	particulate organic carbon	mmolC/m^3
[DIP]	DIP	dissolved inorganic phosphorus	mmolP/m^3
[DOP]	DOP	dissolved organic phosphorus	mmolP/m^3
[POP]	POP	particulate organic phosphorus	mmolP/m^3
[ALK]	Alkalinity	alkalinity	mmol/m^3
[O2]		dissolved oxygen	mmolO$_2$/m^3
T		temperature	°C
PAR		photosynthetical active radiation	µEin/m^2/s
CHLa		total chlorophyll-a	mgCHLa/m^3

Table A1: State and forcing variables

$$\frac{d[Phy1]}{dt} = GPP_{phy1} - MM_{phy1} - EXUD_{phy1} - RR_{phy1} - Graz_{zoo1-phy1}$$

$$\frac{d[Phy2]}{dt} = GPP_{phy2} - MM_{phy2} - EXUD_{phy2} - RR_{phy2} - Graz_{zoo2-phy2}$$

$$\frac{d[Bac]}{dt} = BCP_{bac} - RR_{bac} - MM_{bac} - Graz_{zoo1-bac}$$

$$\frac{d[Zoo1]}{dt} = Graz_{zoo1} - MM_{zoo1} - EXCR_{zoo1} - Graz_{zoo2-zoo1}$$

$$\frac{d[Zoo2]}{dt} = Graz_{zoo2} - MM_{zoo2} - EXCR_{zoo2}$$

$$\frac{d[DIP]}{dt} = -rpc_{phy1} \cdot \left(GPP_{phy1} - RRa_{phy1}\right) - rpc_{phy2} \cdot \left(GPP_{phy2} - RRa_{phy2}\right) - rpc_{bac} \cdot \left(BCP_{bac} - RR_{bac}\right) + Phosp$$

$$\frac{d[DOP]}{dt} = -Phosp + DECA_{POP} + rpc_{zoo1} \cdot EXCR_{zoo1} + rpc_{zoo2} \cdot EXCR_{zoo2} + rpc_{bac} \cdot MM_{bac}$$
$$+ rpc_{phy1} \cdot \left(EXUD_{phy1} + RRb_{phy1}\right) + rpc_{phy2} \cdot \left(EXUD_{phy2} + RRb_{phy2}\right) + CF1_{DOP} + rpc_{bac} \cdot SF1_{bac\_DOC}$$

$$\frac{d[POP]}{dt} = -DECA_{POP} + rpc_{phy1} \cdot MM_{phy1} + rpc_{phy2} \cdot MM_{phy2} + rpc_{zoo1} \cdot MM_{zoo1} + rpc_{zoo2} \cdot MM_{zoo2}$$
$$+ rpc_{phy2} \cdot SF2_{phy2\_POC} + rpc_{zoo1} \cdot SF2_{zoo1\_POC} + rpc_{phy1} \cdot SF1_{phy1\_POC} + sink_{POC} - burialP|_{bottom}$$

$$\frac{d[DIC]}{dt} = -GPP_{phy1} - GPP_{phy2} + RR_{phy1} + RR_{phy2} + RR_{bac} + EXCHair\text{-}sea_{DIC}$$

$$\frac{d[DOC]}{dt} = DECA_{POC} + EXCR_{zoo1} + EXCR_{zoo2} + EXUD_{phy1} + EXUD_{phy2} + MM_{bac} + CF2_{DOC} + SF1_{bac\_DOC} - BCP_{bac}$$

$$\frac{d[POC]}{dt} = -DECA_{POC} + MM_{phy1} + MM_{phy2} + MM_{zoo1} + MM_{zoo2} + SPF1_{phy1\_POC} + SF2_{phy2\_POC}$$
$$+ SF2_{zoo1\_POC} + sink_{POC} - burialC|_{bottom}$$

$$\frac{d[ALK]}{dt} = -rap \frac{d[DIP]}{dt}$$

$$\frac{d[O2]}{dt} = -roc \cdot \frac{d[DIC]}{dt} + EXCHair\text{-}sea_{O2}$$

Table A2. State variable equations.

$GPP_{phyi} = f(T)_{phy} \cdot f(PAR)_{phyi} \cdot f([DIP]) \cdot \mu max_{phyi} \cdot [Phyi]$	Gross primary production of phytoplankton groups, i=1,2

$MM_{phyi} = km_{phyi} \cdot [Phyi]$	Mortality of phytopl. groups, i=1,2
$EXUD_{phyi} = kexud_{phyi} \cdot f(T)_{arrh} \cdot [Phyi]$	Exudation of phytopl. groups, where i=1,2
$RR_{phy\,i} = RRa_{phy\,i} + RRr_{phy\,i}$	Respiration of phytopl. groups, i=1,2
$RRa_{phy\,i} = GPP_{phy\,i} \cdot kra_{phy\,i}$	Active respiration for phytopl. groups, i=1,2
$RRr_{phy\,i} = krr_{phy\,i} \cdot f(T)_{arrh} \cdot [Phy_i]$	Rest respiration for phytopl. groups, i=1,2
$\text{sink}_{phy\,i} = \text{wsink}_{phy\,i} \cdot ([Phy_i]_{up} - [Phy_i]) / dz$	Sinking of phytoplankton groups, i=1,2
$CHLa = \sum_{i=1,2}(0.003 + 0.0154e^{0.050 \cdot T} \cdot e^{-0.059 \cdot PAR} \cdot f([DIP]) \cdot \mu max_{phyi} \cdot [Phyi])$	Carbon to chlorophyll-a conversion (Cloern et al., 1995)

Table A3a. Formulations for Phytoplankton groups.

$BCP_{bac} = f(T)_{bac} \cdot f([DOC])_{bac} \cdot f([DIP])_{bac} \cdot \mu max_{bac} \cdot [Bac]$	Growth of *[Bac]*
$RR_{bac} = kr_{bac} \cdot f(T)_{arrh} \cdot f([O2]) \cdot [bac]$	Respiration of *[Bac]*
$MM_{bac} = km_{bac} \cdot f(T)_{arrh} \cdot (1 - f([O2])) \cdot [bac]$	Lysis of *[Bac]*

Table A3b. Formulations for Bacteria.

$Graz_{zoo1} = eff_{zoo1} \cdot (Graz_{zoo1-phy1} + Graz_{zoo1-bac})$	Growth of *[Zoo1]*
$Graz_{zoo1-ph1} = kgr_{zoo1} \cdot \dfrac{[Phy1]^2}{[Phy1]^2 + [Bac]^2 \cdot Sw_{zoo1}^2 + kf_{zoo1}^2} \cdot [Zoo1]$	Grazing of *[Zoo1]* on *[Phy1]*
$Graz_{zoo1-bac} = kgr_{zoo1} \cdot \dfrac{[Bac]^2 \cdot Sw_{zoo1}^2}{[Phy1]^2 + [Bac]^2 \cdot Sw_{zoo1}^2 + kf_{zoo1}^2} \cdot [Zoo1]$	Grazing of *[Zoo1]* on *[Bac]*
$SF1_{phy1\_POC} = (1 - eff_{zoo1}) \cdot Graz_{zoo1-phy1}$	Sloppy feeding of *[Zoo1]* on *[Phy1]* to POC
$SF1_{bac\_DOC} = (1 - eff_{zoo1}) \cdot Graz_{zoo1-bac}$	Sloppy feeding of *[Zoo1]* on *[Bac]* to DOC
$CF1_{DOP} = (rpc_{bac} - rpc_{zoo1}) \cdot Graz_{zoo1-bac}$	Compensation flux for P:C ratio difference between *[Zoo1]* and *[Bac]*
$Graz_{zoo2} = eff_{zoo2} \cdot \left(Graz_{zoo2-phy2} \cdot \dfrac{rpc_{phy2}}{rpc_{zoo2}} + Graz_{zoo2-zoo1} \right)$	Growth of *[Zoo2]*
$Graz_{zoo2-zoo1} = kgr_{zoo2} \cdot \dfrac{[Zoo1]^2 \cdot Sw_{zoo2}^2}{[Phy2]^2 + [Zoo1]^2 \cdot Sw_{zoo2}^2 + kf_{zoo2}^2} \cdot [zoo2]$	Grazing of *[Zoo2]* on *[Zoo1]*
$Graz_{zoo2-phy2} = kgr_{zoo2} \cdot \dfrac{[Phy2]^2}{[Phy2]^2 + [Zoo1]^2 \cdot Sw_{zoo2}^2 + kf_{zoo2}^2} \cdot [zoo2]$	Grazing of *[Zoo2]* on *[Phy2]*
$SF2_{phy2\_POC} = (1 - eff_{zoo2}) \cdot Graz_{zoo2-phy2}$	Sloppy feeding of *[Zoo2]* on *[Phy2]* to POC
$SF2_{zoo1\_POC} = (1 - eff_{zoo2}) \cdot Graz_{zoo2-zoo1}$	Sloppy feeding of *[Zoo2]* on *[Zoo1]* to POC
$CF2_{DOC} = eff_{zoo2} \cdot Graz_{zoo2-phy2} \cdot \left(1 - \dfrac{rpc_{phy2}}{rpc_{zoo2}} \right)$	Compensation flux for P:C ratio differences between *[Zoo2]* and *[Phy2]*
$MM_{zoo\,i} = Km_{zoo\,i} \cdot [Zoo_i]$	Mortality of zoopl.s., i=1,2
$EXCR_{zoo\,i} = Kexcr_{zoo\,i} \cdot f(T)_{arrh} \cdot [Zoo_i]$	Excretion of zoopl.s., i=1,2

Table A3c. Formulations for zooplankton groups.

$Phosp = v_{phosp} \cdot f([DOP]) \cdot f([DIP]) \cdot f(T)_{arrt} \cdot [Bac]$	Phosphorus remineralization via phosphatase
$DECA_{POC} = kdec_{POC} \cdot f(T)_{arrh} \cdot f([POC])_{POC} \cdot [POC]$	Decay of POC
$DECA_{POP} = kdec_{POP} \cdot f(T)_{arrh} \cdot f([POP])_{POP} \cdot [POP]$	Decay of POP
$burialP\big|_{bottom} = kburial_{POP} \cdot [POP]_{bottom}$	Burial of POP at the bottom layer
$burialC\big|_{bottom} = kburial_{POC} \cdot [POC]_{bottom}$	Burial of POC at the bottom layer
$\text{sink}_{POP} = \text{wsink}_{pop} \cdot ([POP]_{up} - [POP]) / dz$	Sinking of POP
$\text{sink}_{POC} = \text{wsink}_{poc} \cdot ([POC]_{up} - [POC]) / dz$	Sinking of POC

Table A3d. Formulations for DOC, DOP, POC and POP.

$$f(T)_{arrh} = 10^{(20-T)}$$ Arrhenius formulation - Q_{10}

$$f(T)_{phyi} = \left[\frac{(T\max_{phyi} - T)}{(T\max_{phyi} - Topt_{phyi})}\right]^{Coeff_{phyi} \cdot (T\max_{phyi} - Topt_{phyi})}$$

Lassiter and Kearnel formulation, i =1,2
Same formulation is applied to bacteria

$$\cdot e^{coeff_{phyi} \cdot (T - Topt_{phyi})}$$

$$f(PAR)_{phyi} = \frac{PAR_k}{PARopt_{phyi}} \cdot e^{\frac{PAR_k}{PARopt_{phyi}}}$$ Steele formulation, i =1,2 at the level k

$$PAR_k = PAR_0 \cdot e^{\int_0^k (kest + kest_{phy1} \cdot [Phy1]_{k-1} + kest_{phy2} \cdot [Phy2]_{k-1})dz}$$

Light at the depth level k. Attenuation of light along water column and self shading.

$$PAR_0 = par_{conv} \cdot par_{frac} \cdot Qsw$$ Conversion from Short wave [W/m^2] radiation to PAR

$$f([DOC])_{bac} = \frac{[DOC]}{[DOC] + k_{DOC}}$$ Monod formulation for DOP in bacteria phosphatase

$$f([DOP])_{phosp} = \frac{[DOP]}{[DOP] + k_{DOP}}$$ Monod formulation for DOC in bacteria growth

$$f([DIP])_{phyi} = \frac{[DIP]}{[DIP] + kdip_{phyi}}$$ Monod formulation for P in phytoplankton growth, i =1,2

$$f([DIP])_{bac} = \frac{[DIP]}{[DIP] + kdip_{bac}}$$ Monod formulation for P in bacteria growth

$$f([O2])_{bac} = \frac{[O2]}{[O2] + ko2}$$ Monod formulation for O$_2$ in bacteria growth

$$f([POC])_{POC} = \frac{[POC]}{[POC] + k_{POC}}$$ Monod formulation for POC

$$f([POC])_{POP} = \frac{[POP]}{[POP] + k_{POP}}$$ Monod formulation for POP

$EXCHair\text{-}sea_{O2}$ Air-sea exchange, formulation as in Solidoro et al., 2005

$EXCHair\text{-}sea_{DIC}$ Air-sea exchange, formulation as in Follow et al., 2006

Table A3e. Functional equations

Parameter	Unit	Value	name	
μmax_{phy1}	[d^{-1}]	3.6	Maximum growth rate for *[Phy1]*	*
$Tmax_{phy1}$	[°C]	31	Max temp. for *[Phy1]*	
$Topt_{phy1}$	[°C]	23	Optimal temp. for *[Phy1]*	
$coeff_{phy1}$	[-]	0.1157	Exponential coeff. in T formulation for *[Phy1]*	
$PARopt_{phy1}$	[µEin/m^2/s]	400	Optimal irradiance for *[Phy1]*	*
$Kdip_{phy1}$	[mmol P/m^3]	0.05	Half saturation in P Monod formulation for *[Phy1]*	
$kexud_{phy1}$	[d^{-1}]	0.072	Exudation rate for *[Phy1]*	
km_{phy1}	[d^{-1}]	0.096	Mortality rate for *[Phy1]*	
rpc_{phy1}	[molP/molC]	0.00943	P:C ratio of *[Phy1]*	
kra_{phy1}	[-]	0.08	Active respiration fraction for *[Phy1]*	(4)
krr_{phy1}	[d^{-1}]	0.06	Basal specific respiration rate for *[Phy1]*	(4)
$wsink_{phy1}$	[m/d]	0.5	sinking rate for *[Phy1]*	
μmax_{hphy2}	[d^{-1}]	6	Maximum growth rate for *[Phy2]*	*
$Tmax_{phy2}$	[°C]	35	Max temp. for *[Phy2]*	
$Topt_{phy2}$	[°C]	18	Optimal temp. for *[Phy2]*	
$coeff_{phy2}$	[ ]	0.05	Exponential coeff. in T formulation for *[Phy2]*	
$PARopt_{phy2}$	[µEin/m^2/s]	300	Optimal irradiance for *[Phy2]*	*
ksp_{phy2}	[mmol P/m^3]	0.15	Half saturation in P Monod formulation for *[Phy2]*	
$kexud_{phy2}$	[t^{-1}]	0.03	Exudation rate for *[Phy2]*	
km_{phy2}	[t^{-1}]	0.12	Mortality rate for *[Phy2]*	

rpc$_{phy2}$	[molP/molC]	0.008	P:C ratio for *[Phy2]*	
kra$_{phy2}$	[d^{-1}]	0.15	Active respiration fraction for *[Phy2]*	(4)
krr$_{phy2}$	[-]	0.06	Basal specific respiration rate for *[Phy2]*	(4)
wsink$_{phy2}$	[m/d]	1.0	sinking rate for *[Phy2]*	
μmax$_{bac}$	[d^{-1}]	1.2	Maximum growth rate for *[bac]*	
Tmax$_{bac}$	[°C]	40	Max temp. for *[bac]*	
Tott$_{bac}$	[°C]	26	Optimal temp. for *[bac]*	
coeff$_{bac}$	[ ]	0.1157	Exponential coeff. in T formulation for *[bac]*	
kdoc$_{bac}$	[ ]	10	Half saturation in DOC Monod formulation for *[bac]*	
kdip$_{bac}$	[mmol P/m^3]	0.02	Half saturation in P Monod formulation for *[bac]*	
kr$_{bac}$	[d^{-1}]	0.4	Respiration rate for *[bac]*	
km$_{bac}$	[d^{-1}]	0.6	Lysis rate for [bac]	
rpc$_{bac}$	[molP/molC]	0.02	P:C ratio for *[bac]*	
kgr$_{zoo1}$	[d^{-1}]	2.16	Grazing rate for *[zoo1]*	
kf$_{zoo1}$	[mmol C/m^3]	10	Half saturation of grazing for *[zoo1]*	
eff$_{zoo1}$	[ ]	0.7	Assimilation efficiency of *[zoo2]* on *[Phy2]*	
km$_{zoo1}$	[d^{-1}]	0.36	Mortality rate for *[zoo1]*	
kexcr$_{zoo1}$	[d^{-1}]	0.12	Excretion rate for *[zoo1]*	
rpc$_{zoo1}$	[molP/molC]	0.00833	P:C ratio for *[zoo1]*	
Sw$_{zoo1}$	[ ]	2	Diet coefficient of *[zoo1]*	
kgr$_{zoo2}$	[d^{-1}]	1.2	Grazing rate for *[zoo2]*	
kf$_{zoo2}$	[mmol C/m^3]	17.3	Half saturation of grazing for *[zoo2]*	
eff$_{zoo2}$	[ ]	0.7	Assimilation efficiency of *[zoo2]*	
km$_{zoo2}$	[d^{-1}]	0.072	Mortality rate for *[zoo2]*	
kex$_{zoo2}$	[d^{-1}]	0.048	Excretion rate for *[zoo2]*	
rpc$_{zoo2}$	[molP/molC]	0.00878	P:C ratio for *[zoo2]*	
Sw$_{zoo2}$	[ ]	1.5	Diet coefficient of *[zoo2]*	
wsink$_{POP}$	[m/d]	1	sink rate for *[POP]*	
kburial$_{POP}$	[d^{-1}]	0.0025	burial rate for *[POP]*	
kdec$_{POP}$	[d^{-1}]	0.06	Decay rate of *[POP]*	
k$_{POP}$	[mmol P/m^3]	0.02	half saturation for *[POP]*decay	
k$_{DOP}$	[mmol P/m^3]	0.15	Half saturation of P for alkaline phosphatase	*
v$_{phosp}$	[d^{-1}]	0.02	Max rate of phosphatase	*
wsink$_{POC}$	[m/d]	2.5	sink rate for *[POC]*	
kburial$_{POC}$	[d^{-1}]	0.0025	burial rate for *[POC]*	
k$_{POC}$	[mmol C/m^3]	2	half saturation for *[POC]* decay	
kdec$_{POC}$	[d^{-1}]	0.04	Decay rate of *[POC]*	*
kest$_{phy1}$	[m^2/mmol C]	0.04	Extinction factor due to *[Phy1]*	(2)
kest$_{phy2}$	[m^2/mmol C]	0.04	Extinction factor due to *[Phy2]*	(2)
kest	[m^{-1}]	0.04	Extinction coefficient of sea water	(2)
Par$_{conv}$	[μEin/m^{2}s]/[W/m^2]	1/0.2174	Qsw to PAR conversion factor	
Par$_{frac}$	[-]	0.4	Fraction of active photosynthetic radiation	
Rap	[molALK/molP]	21.8	Phosphorus to alkalinity factor	(3)
Roc	[molO2/molC]	0.5	Carbon to oxygen conversion	
ko2	[mmolO2/m^3]	90	half saturation of O2	

Table A4. Model parameters as in Cossarini and Solidoro (2008). Last column indicates changed parameters: * estimated in the present work; [1] from Solidoro et al., (2005); [2] from Kremer and Nixon (1978); [3] from Wolf-Gladrow et al., (2007); [4] from Lazzari et al., (2012).

References:

Adcroft, A., Campin, J-M., Dutkiewicz, S., Evangelinos, C., Ferreira, D., Forget, G., Fox-Kemper, B., Heimbach, P., Hill, C., Hill, E., Hill, H., Jahn, O., Losch, M., Marshall, J., Maze, G., Menemenlis, D., Molod, A.: MITgcm User Manual, MIT Department of EAPS, Cambridge, MA, US, 2011.

Butenschön, M., Zavatarelli, M., Vichi, M.: Sensitivity of a marine coupled physical biogeochemical model to time resolution, integration scheme and time splitting method, Ocean Modelling, 52–53, 36–53, 2012.

Cloern, J.E., Grenz, C., Vidergar-Lucas, L.: An empirical model of the phytoplankton chlorophyll: carbon ratio-the conversion factor between productivity and growth rate, Limnol. Oceanogr., 40(7), 1313-1321, 1995.

Cossarini, G., and Solidoro, C.: Global sensitivity analysis of a trophodynamic model of the gulf of Trieste, Ecological modelling, 212, 16-27, doi:10.1016/j.ecolmodel.2007.10.009, 2008.

Cossarini, G., Solidoro, C., Fonda Umani, S.: Dynamics of biogeochemical properties in temperate coastal areas of freshwater influence: lessons from the Northern Adriatic Sea (Gulf of Trieste), Estuarine, Coastal and Shelf Science, 115, 63-74, 2012

Cushing, D.H.: A difference in structure between ecosystems in strongly stratified waters and in those that are only weekly stratified, Journal of Plankton Research, 11(1), 1-13, 1989.

Follows, M.J., Ito, T., Dutkiewicz, S.: On the solution of the carbonate chemistry system in ocean biogeochemistry models, Ocean Modelling, 12, 290-301, 2006.

Hoppe, H.G.: Phosphatase in the sea, Hdrobiologia, 493, 187-200, 2003.

Labry, C., Delmas, D., and Herbland, A.: Phytoplankton and bacterial alkaline phosphatase activities in relation to phosphate and DOP availability within the Gironde plume waters (Bay of Biscay), Journal of experimental marine biology and ecology, 318(2), 213-225, 2005.

Lazzari, P., C. Solidoro, V. Ibello, S. Salon, A. Teruzzi, K. Béranger, S. Colella, Crise A.: Seasonal and inter-annual variability of plankton chlorophyll and primary production in the Mediterranean Sea: a modelling approach, Biogeosciences, 9(1), 217–233, doi:10.5194/bg-9-217-2012, 2012.

Legendre, L. Rassoulzadegan, F.: Plankton and nutrient dynamics in marine water, Ophelia, 41, 153-172, 1995.

Kremer, J.N., Nixon, S.W.: A coastal marine ecosystem. Simulation and analysis. Springer-Verlag, Berlin, 1978.

Marshall, J.C., Adcroft, A., Hill, C., Perelman, L. and Heisey, C.: A finite-volume, incompressible Navier-Stokes model for the studies of the ocean on parallel computers, J. Geophys. Res., 102: 5753-5766, 1997.

Orr, J.C., Najjar, R., Sabine, C.L., Joos, F.: Abiotic HOWTO. Internal OCMIP Report, LSCE/CEA Saclay, Gifsur-Yvette, France, 1999.

Querin, S., Cossarini, G., and Solidoro, C.: Simulating the formation and fate of dense water in a mid-latitude marginal sea during normal and warm winter conditions. Submitted to J. Geophys. Res.-Oceans, 2012.

Solidoro, C, Pastres, R, Cossarini, G.: Nitrogen and plankton dynamics in the Venice lagoon. Ecol Model, 184 103–124, 2005.

Wolf-Gladrow, D.A., Zeebe, R.E., Klaas, C., Körtzinger, A., and Dickson, A.G.: Total alkalinity: The explicit conservative expression and its application to biogeochemical processes, Marine Chemistry, 106, 287–300, 2007.

CO2 exchange in a temperate marginal sea of the Mediterranean Sea: processes and carbon budget

G. Cossarini, S. Querin, C. Solidoro

Appendix B: Model validation

The validation of a complex ecosystem model representing a heterogeneous domain (like the Adriatic Sea) is far from being a trivial task. Beside the fact that the discussion on indicators and metrics for the assessment of model skill is still debated, a proper validation of a 3D biogeochemical dynamic model would require a dataset that covers the annual cycle of the simulated variables and that resolves the horizontal gradients and vertical profiles for all the relevant physical, chemical and biological variables simulated. The spatial and temporal coverage of observations and model output should match – at least to some extent- in order to apply the standard skill assessment methods. Unfortunately, a dataset that meets these criteria is seldom available and it is not available for the Adriatic Sea. The lack of a suitable validation dataset is particularly significant for the carbonate system variables. Therefore, a model corroboration has been performed considering a flexible approach by i) assessing the skill of the model against existing datasets, and ii) assessing the consistency of the model against climatological datasets, literature data and estimates, in case no other information is available.

In particular, MODIS satellite data for chlorophyll-a from April 2007 to December 2008 (Volpe et al., 2012) has been used to assess the skill of the model in simulating trends and surface gradients of the phytoplankton biomass. Three climatological datasets (Zavatarelli et al., 1998, Solidoro et al., 2009, Cossarini et al., 2012) have been used to validate 1) the seasonal dynamics, 2) the vertical differences and 3) the spatial gradients of DIP, dissolved oxygen and chlorophyll-a in different areas. Literature data has been used to assess the consistency of the model in simulating relevant ecosystem processes (e.g.: primary and bacterial production, sinking rate) and other relevant variables (DOP, pCO_2, DIC and alkalinity).

B1 Chlorophyll-a dynamics

Considering the chlorophyll-a observations in the Adriatic Sea, the main features are the presence of an eutrophic zone along the Italian coast and generally low chlorophyll levels over the rest of the basin. The trophic frontal system is triggered by the input of water and nutrients from the Po River and the other rivers on the north-western part the Adriatic Sea. The extension and intensity of the eutrophic strip is modulated by the seasonality of river inputs and by the oceanographic dynamics, thus, it is highly variable in time. The northern sub-basin (NA) presents higher chlorophyll content than the central (CA) and southern (SA) ones, also because of the recirculation processes that move Po waters towards the centre of the NA (Zavaterelli et al., 1998, Solidoro et al., 2009, Mozetic et al., 2009). A few local coastal hot spots of high chlorophyll-a concentrations are detectable along the south-eastern coast, where several rivers supply nutrients to the coastal area that is generally influenced by the oligotrophic waters entering from the Ionian Sea (Marini et al., 2010). During winter, the central part of the SA is characterized by high values of surface chlorophyll-a; the productivity of this area is triggered by open ocean convection events (Batistić et al., 2011).

Model chlorophyll-a results are compared with monthly MODIS satellite chlorophyll-a maps in Fig. B1. MODIS data are provided by the MyOcean system (Volpe et al., 2012),. Chlorophyll-a has been estimated from the modelled biomass of the two phytoplankton groups using the formulation by Cloern et al. (1995), which takes into account light availability, temperature and growth rate (see Appendix A). For the comparison, the modelled chlorophyll-a has been averaged on the e-folding depth of PAR.

A further quality check has been performed by comparing the temporal trend of the simulated surface chlorophyll-a concentration for the three sub-basins, with the monthly box-plots of MODIS data (as represented in Figure B2). Results of the application of several skill assessment indexes (listed in Tab. B1) are reported in Fig. B3. The indexes are calculated for the three sub-basins for each couple of model-satellite monthly map.

Finally, simulated seasonal vertical profiles of chlorophyll-a have been compared with climatological data (Solidoro et al., 2009) for two areas (coastal and offshore) in the NA (Fig. B4).

Bias	Root Mean Square of the differences
$bias = \frac{1}{np} \sum \text{mod} - \text{sat}$	$rms = \sqrt{\frac{1}{np} \sum (\text{mod} - \text{sat})^2}$
Nash Sutcliffe Model Efficiency	Correlation index
$ME = 1 - \dfrac{\sum (\text{mod} - \text{sat})^2}{\sum (\text{sat} - \overline{\text{sat}})^2}$	$corr = \dfrac{\sum (\text{mod} - \overline{\text{mod}}) \cdot (\text{sat} - \overline{\text{sat}})}{\sqrt{\sum (\text{mod} - \overline{\text{mod}})^2 \cdot \sum (\text{sat} - \overline{\text{sat}})^2}}$
ROC (relative operating characteristic) index (Beck and Shultz, 1986; Fielding and Bell, 1997; Sheng and Kim, 2009; Wiley et al., 2003).	
The presence of a satellite bloom is compared with the model results by counting the grid-points where the model correctly simulates the observed bloom - true positive (TP) -, and the grid-points where the model correctly reproduces the absence of the bloom - true negative (TN). In the ROC sensitivity index, the number of true positive cases is compared with the total number of satellite bloom cases (solid lines *vs* dashed lines in Fig. B3). In the ROC specificity index, the number of true negative cases is compared with the total number of bloom absence gridpoints in satellite data (solid lines *vs* dashed lines in Fig. B3). A threshold of 0.3 mg/m^3 (which corresponds to the 75th percentile of the distribution of satellite values) is used for assessing the presence of surface bloom.	

Tab.B1. Indexes used for the comparison between model and satellite monthly surface chlorophyll-a maps.

The qualitative comparison between monthly maps (Fig. B1) shows that the model reproduces the relevant features characterizing the spatial distribution and temporal dynamics of surface chlorophyll-a in the Adriatic Sea. In particular, the observed high chlorophyll-a concentrations in the NA and CA (i.e.: along the Italian coast) and the oligotrophic conditions of the rest of the basin are well simulated. In particular the model reproduces the role of the western Adriatic current (WAC) in confining the nutrients rich waters discharged by the Po river within a narrow coastal strip (Fig. B1).

The modelled chlorophyll-a gradient from NA to CA, observed in autumn and winter satellite maps, is caused by the simulated recirculation dynamics within the NA (Querin et al., 2012) and by the higher nutrient availability caused by higher nutrient remineralization (see DIP profiles). The model underestimates the chlorophyll-a concentration in the NA in November and December 2007 and February 2008, probably due to the underestimation of the nutrient input from the minor rivers (whose discharge rates are derived from a climatological dataset, with a modulation that roughly mimic the seasonal cycle (Querin et al., 2012)).

Trends of median and quartiles of chlorophyll-a observations are fairly well resolved by the model (Fig. B2), thus highlighting its capability in simulating the temporal variability of the extension of the frontal system as a function of the seasonal variation of nutrient discharges and of the temporal variation of the physical dynamics. The good model performance in reproducing the observed spatial patterns of NA and CA are quantitatively assessed by the high values of correlation (higher than 0.60 for most of the months, Fig. B3), of ROC sensitivity (higher than 50%, Fig. B3) and of ROC specificity (generally higher than 90%, Fig. B3). The two ROC indexes assess the capability of the model to capture the spatial shape of the bloom areas.

In the CA, BIAS and RMS are low and the ME index shows values higher than 0 for most of the months. Only spring ME values are lower than 0 (values lower than 0 are reported as 0 in Fig. B3) indicating a lower performance of the model in this period (see also the low values of correlation in Fig. B3). An overestimation of the vertical mixing of nutrient in the central part of the CA causes the mismatch of surface patterns between model and satellite data.

The comparison between simulated and climatological chlorophyll-a vertical profiles for the coastal area of NA in each season (Fig. B4) shows the capability of the model to reproduce the observed vertical processes and to simulate the seasonal cycle also in the eutrophic coastal area. The observed higher values of chlorophyll-a at the deepest layers of the offshore area (area 11 in Fig. B4) during summer are reproduced by the model that, therefore, correctly simulates the fertilization effect driven by nutrient remineralization of the organic matter accumulated on the bottom. The coast-to-offshore gradient is also simulated by the model (Fig. B4) that, however, underestimates the chlorophyll-a values at surface over the offshore area.

Other skill indexes (Figure B3) show that NA is characterized by a negative BIAS for the autumn and winter months. For these months the ROC sensitivity (Fig. B3) shows the lowest agreement between simulated and observed blooms. The model underestimation mainly regards the third and fourth quartiles (Fig. B2), which correspond to very coastal areas, where satellite estimations are known to have the largest uncertainties.

Concerning the SA, the sequence of maps of Fig. B1 shows that the general oligotrophic conditions are well simulated by the model (low BIAS and RMS and high ROC specificity for most of the months in Fig. B3). In the central part of SA, the timing and values of the winter bloom are well simulated by the model (maps of Fig. B1, trend in Fig. B2 and ROC sensitivity in Fig. B3). The simulated dynamics of the surface fertilization and of the subsequent formation of the deep chlorophyll maximum (Section 3.2 and Fig. 5 in the manuscript) is consistent with this feature frequently observed in the SA (Boldrin et al., 2002). The spatial extension of the simulated bloom is slightly overestimated, as highlighted by the low ROC specificity (high difference between solid and dashed lines) and by the high BIAS for March 2008 (Fig. B3). Coastal chlorophyll-a hot spots in the eastern part of SA (Fig. B1), driven mainly by local river input, are consistent with satellite maps (Fig. B1) and results reported by Marini et al. (2010). Very low chlorophyll-a concentrations and lack of strong spatial patterns for most of the months highlight that ME and correlation are less effective in the skill assessment (Fig. B3).
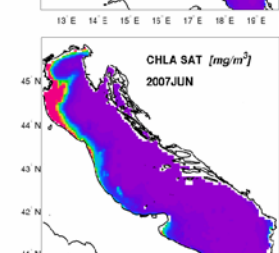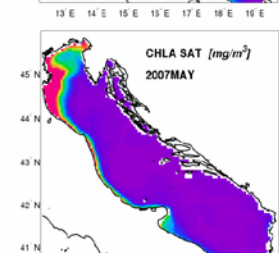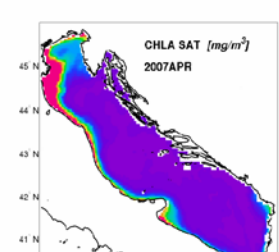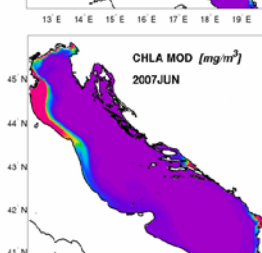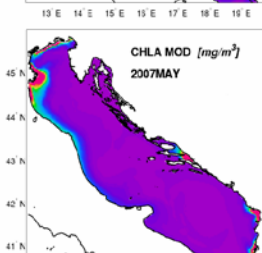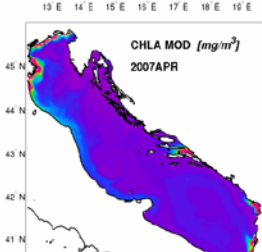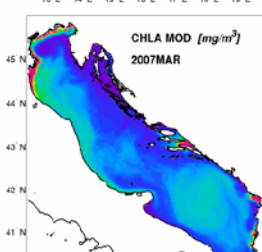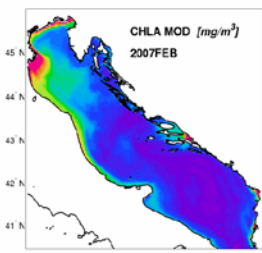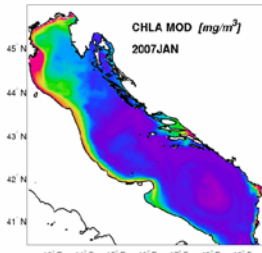
2007 Model Modis | 2008 Model Modis
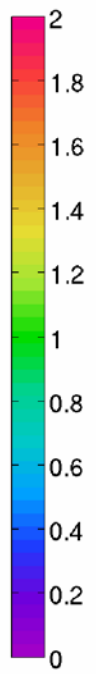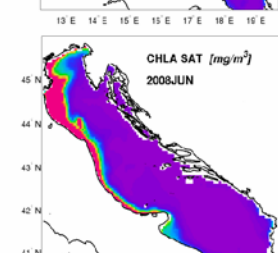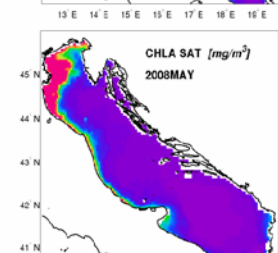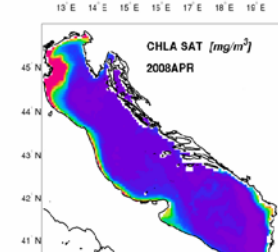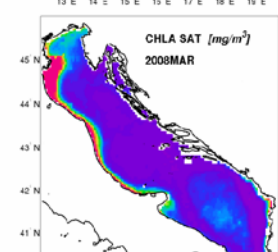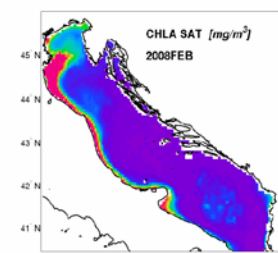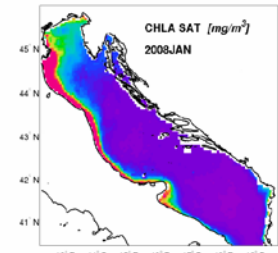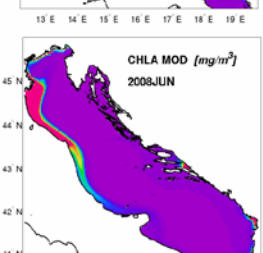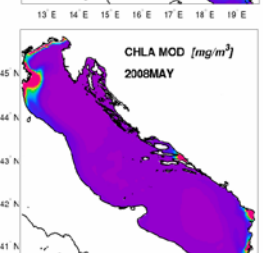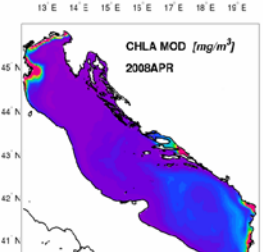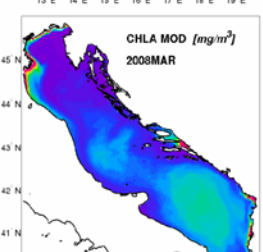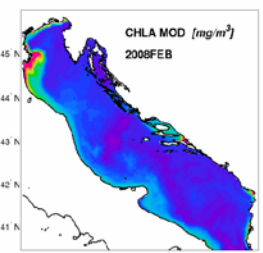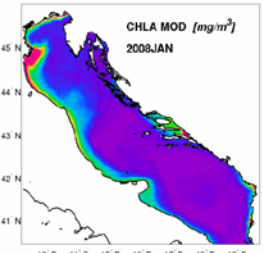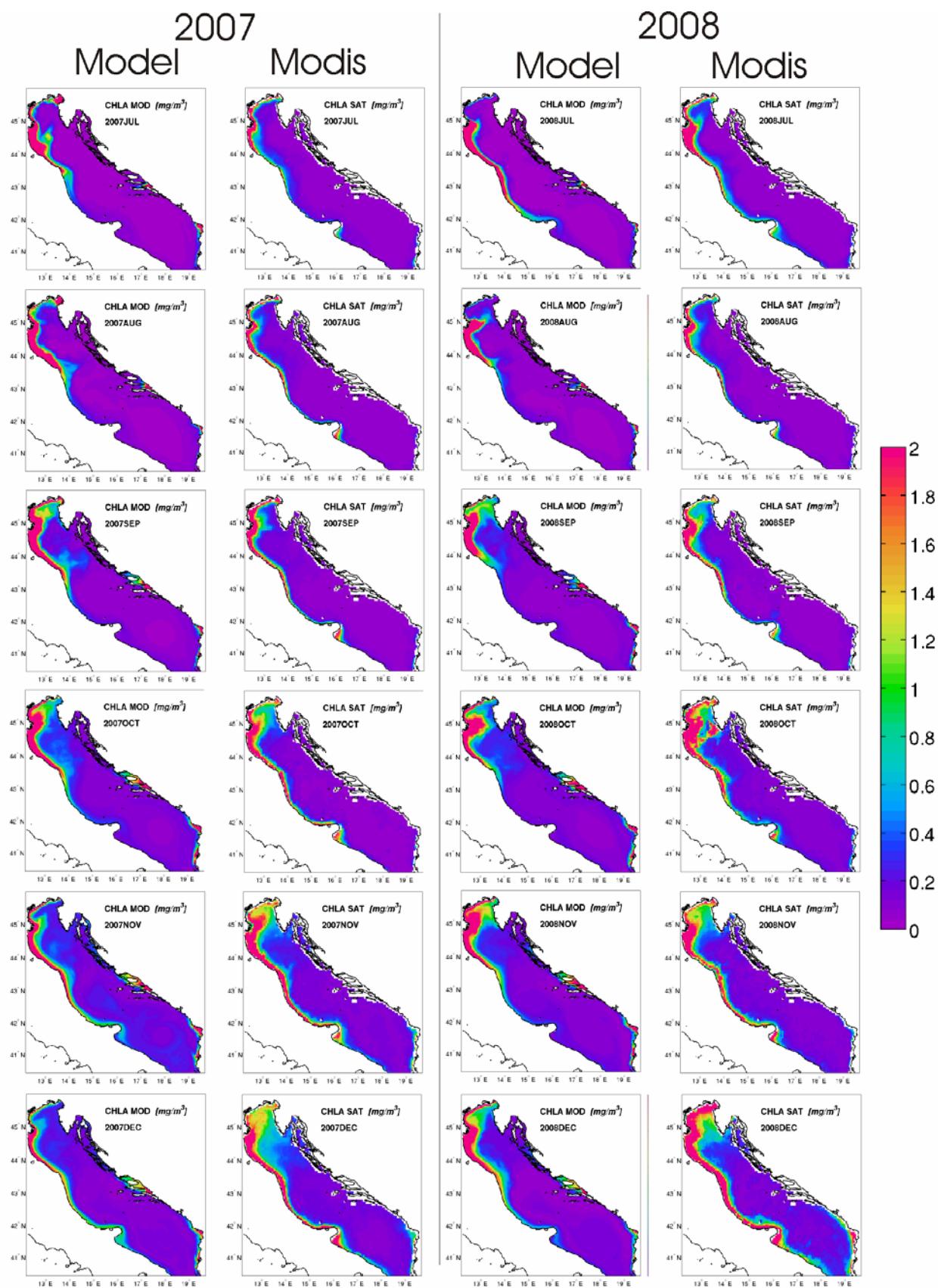
Fig. B1: monthly maps of surface chlorophyll-a derived from the model simulation (first and third columns) and from MODIS satellite data (second and fourth columns), for 2007 (left group) and 2008 (right group). MODIS data for January, February and March 2007 are not available.
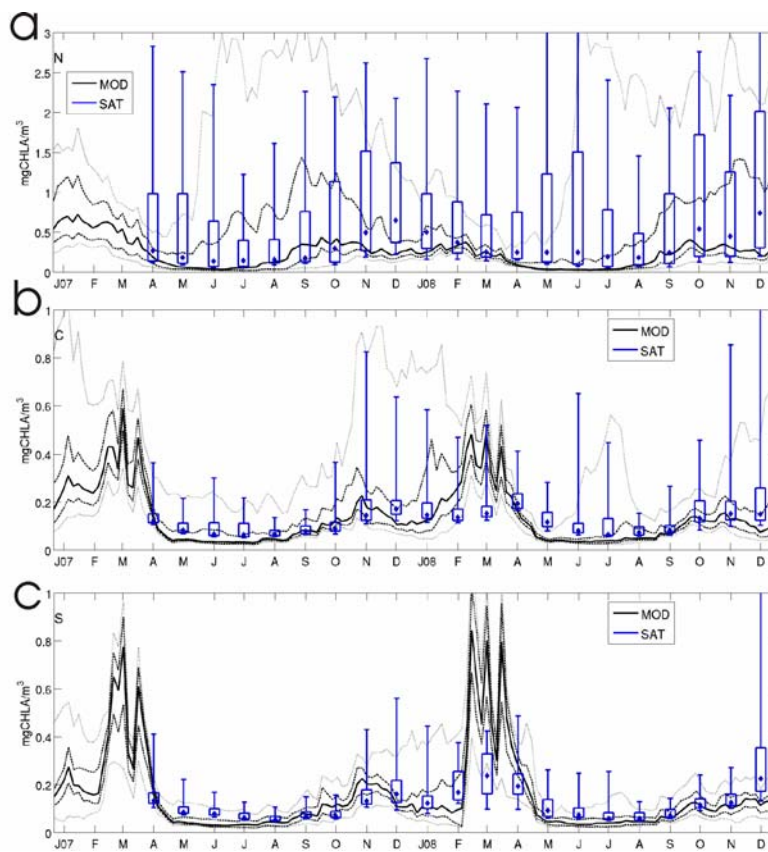
Fig. B2: trend of simulated chlorophyll-a (black lines) and satellite chlorophyll-a (blue boxplots) for the northern (A), central (B) and southern (C) Adriatic sub-basins. The black lines (black solid lines, black dotted lines and grey lines) and the boxplots (dots, boxes and whiskers) report median, interquartile (IQR) and min-max ranges, respectively.
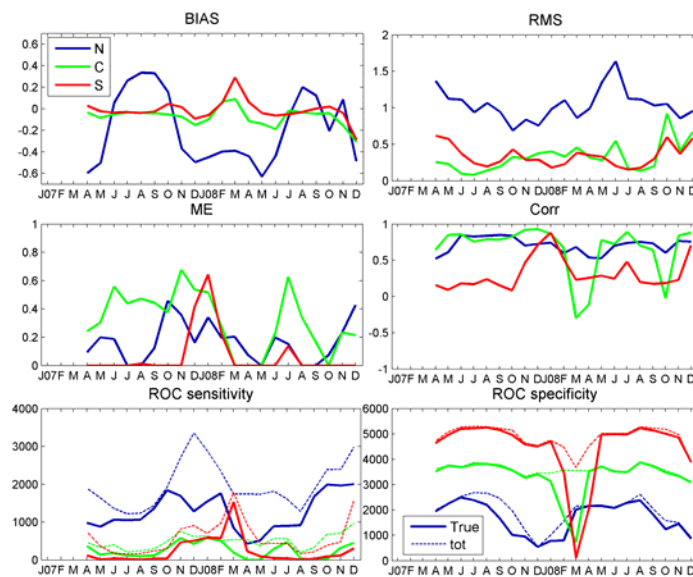
Fig. B3: time series of the skill assessment indexes (see table B1 for their description). For the two ROC indexes the plots report the total number of satellite grid-points that satisfy the bloom threshold and the no-bloom conditions (dashed lines) and the number of true simulated grid-points (solid lines).
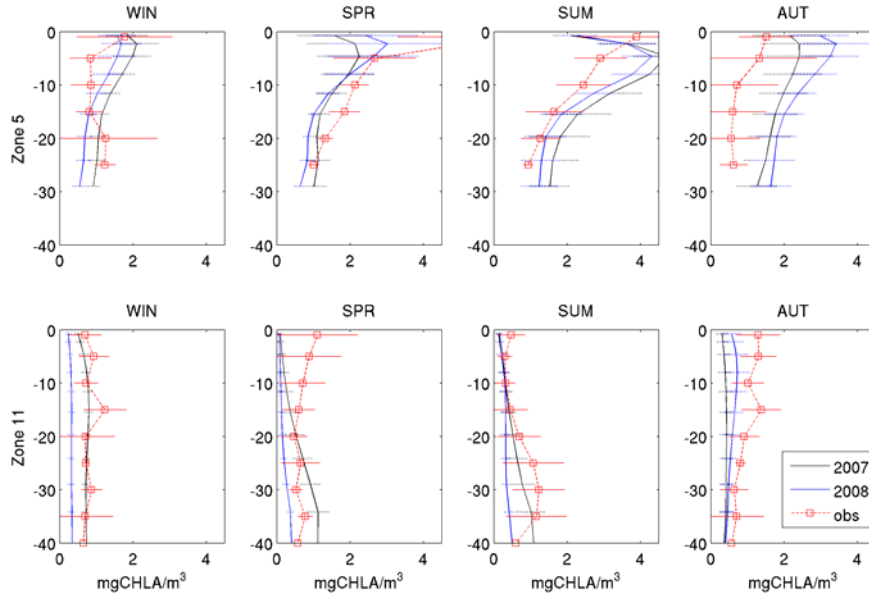
Fig. B4: Mean seasonal profiles of Chlorophyll-a for selected areas in the northern Adriatic Sea defined in Solidoro et al. (2009): a shallow coastal area influenced by Po river discharge (Zone5, upper plots) and an offshore area (Zone11, lower plots). Horizontal lines report the range mean±standard deviation for observations and model results.

B.2. DIP dynamics

The validation of simulated DIP, shown in Fig. B5 and Tab. B2, is performed on a seasonal basis using three climatologies of different areas: the CA and SA together (Zavaterelli et al., 1998), the NA (Solidoro et al., 2009) and the northernmost part of the Adriatic Sea (Cossarini et al., 2012).

The observed coastal-to-offshore negative gradient in the NA is consistently reproduced by the model (Fig. B5). The nutrient discharges from the Po River and the simulated physical dynamics correctly represents the eutrophic coastal strip as described in the previous sections. In fact, within the eutrophic coastal area the model satisfactorily simulates the surface seasonal cycle, whereas the simulated sub-surface values are within the range of the observed ones (Fig. B5). The model reproduces the accumulation of organic matter at the bottom and the subsequent mineralization that stimulates local phytoplankton blooms during summer, as previously shown. In particular, the summer and autumn accumulation at the bottom is qualitatively reproduced by the model in the offshore area (Fig. B5), although, at surface, the model shows a general underestimation of DIP, possibly caused by too fast nutrient uptake kinetics.

In the CA and SA, the model reproduces fairly well the seasonal patterns characterized by higher values in winter and autumn and lower values in summer (Tab. B2). Observed DIP values at the bottom are higher than at the surface, and DIP data show the tendency of accumulation during summer and autumn; these features are satisfactorily simulated by the model. However, also for the CA and SA, the model underestimates the surface summer and spring values.

Deviations from observations are recognizable on the bottom of the Gulf of Trieste area, highlighting a possible underestimation of the bottom remineralization processes in this very shallow area. Furthermore, the model has only a simple parameterization of benthic-pelagic coupling processes (sunk material, accumulated over the sediment, is partially buried, and partially mineralized as a function of temperature, bacteria and oxygen availability) that might be inadequate for very shallow areas. However, the very high values of standard deviation of observations suggest that this restricted area may be characterized by local and coastal dynamics that cannot be resolved at the spatial resolution of our model.
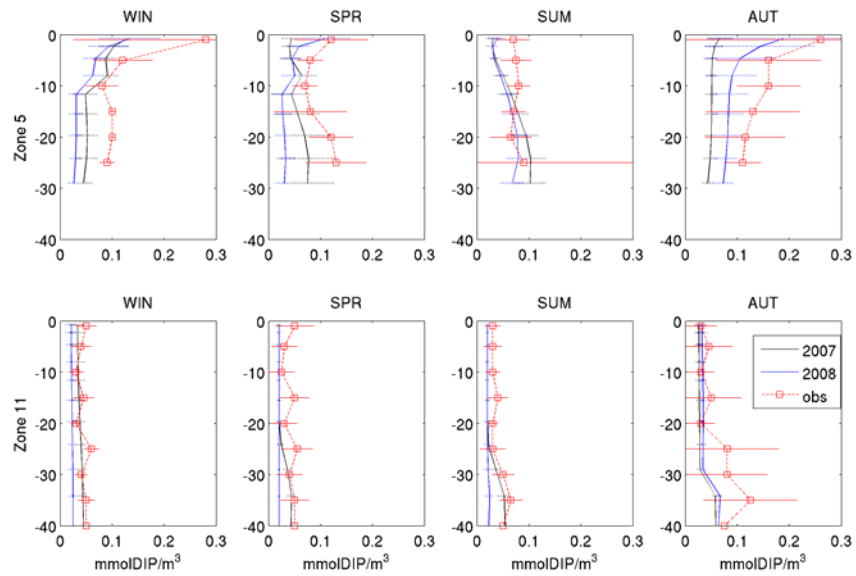
Fig. B5. Mean seasonal profiles of DIP for selected areas in the northern Adriatic Sea defined in Solidoro et al., (2009): a shallow coastal area influenced by Po river discharge (Zone5, upper plots) and an offshore area (Zone11, lower plots). Horizontal lines report the range mean±standard deviation for observations and model results.

Areas	Season	observations	Model 2007	Model 2008
CA, surface water [1]	Win	0.07±0.02	0.05±0.04	0.05±0.04
	Spr	0.07±0.03	0.01±0.04	0.01±0.04
	Sum	0.06±0.03	0.01±0.03	0.01±0.03
	Aut	0.06±0.03	0.04±0.04	0.03±0.04
CA, deep water [1]	Win	0.11±0.05	0.11±0.03	0.09±0.01
	Spr	0.11±0.07	0.11±0.02	0.09±0.01
	Sum	0.11±0.05	0.14±0.01	0.12±0.01
	Aut	0.13±0.05	0.15±0.01	0.14±0.01
SA, surface water [1]	Win	0.06±0.03	0.08±0.02	0.09±0.02
	Spr	0.06±0.03	0.01±0.01	0.01±0.00
	Sum	0.04±0.03	0.01±0.01	0.01±0.00
	Aut	0.06±0.06	0.04±0.02	0.03±0.01
SA, deep water [1]	Win	0.08±0.03	0.12±0.01	0.12±0.01
	Spr	0.07±0.03	0.12±0.01	0.13±0.01
	Sum	0.08±0.03	0.13±0.01	0.14±0.01
	Aut	0.11±0.07	0.14±0.01	0.14±0.01
Gulf of Trieste, surface [2]	Win	0.06±0.06	0.04±0.02	0.03±0.03
	Spr	0.07±0.09	0.01±0.00	0.01±0.01
	Sum	0.05±0.05	0.02±0.00	0.01±0.00
	Aut	0.07±0.05	0.04±0.01	0.05±0.04
Gulf of Trieste, bottom [2]	Win	0.06±0.05	0.07±0.04	0.02±0.01
	Spr	0.07±0.06	0.04±0.01	0.02±0.01
	Sum	0.12±0.14	0.08±0.02	0.02±0.02
	Aut	0.11±0.10	0.04±0.01	0.06±0.03
central part of CA, surface [3]	Annual mean	<0.06	0.03±0.03	0.03±0.04
central part of CA, bottom [3]	Annual mean	0.09	0.11±0.03	0.10±0.02

Tab. B2. Seasonal mean and standard deviation of DIP for selected areas. Data derive from [1] Zavatarelli et al., 1998, [2] Cossarini et al., 2012, [3]Fig. 3 of Vilibic et al., 2012.

B.3. Dissolved oxygen dynamics

Mean seasonal profiles of dissolved oxygen are reported in Fig. B6. Model reproduces fairly well the seasonal cycle and the vertical profiles, indicating that the overall dynamics of production and consumption of oxygen are, at least qualitatively, well reproduced.

The main differences between model and observation are registered for the bottom values of the coastal area during summer and autumn. The model, which lacks of an explicit benthic model, might underestimate the benthic respiration for the very coastal areas.
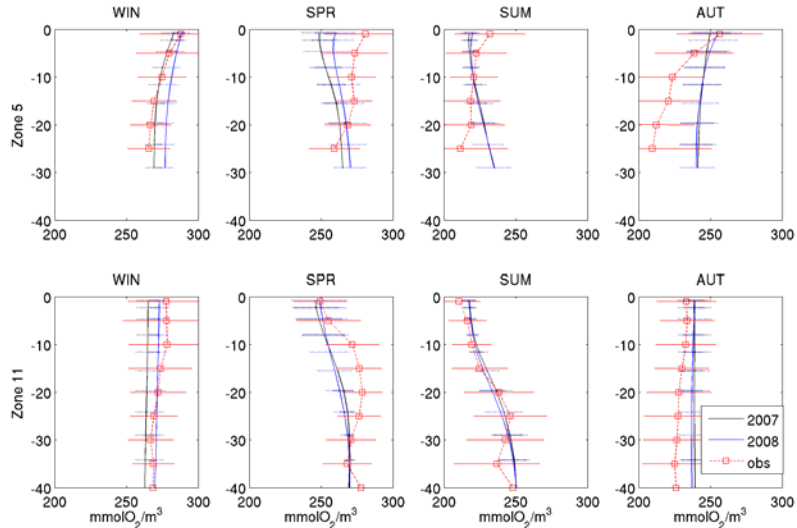
Fig. B6. Mean seasonal profiles of dissolved oxygen for selected areas in the northern Adriatic Sea defined in Solidoro et al., (2009): a shallow coastal area influenced by Po river discharge (Zone5, upper plots) and an offshore area (Zone11, lower plots). Horizontal lines report the range of mean±standard deviation for observations and model results.

B.4. DOP dynamics

The DOP represents a large reserve of phosphorus, as important as the DIP, in the marine ecosystems (Karl and Björkman, 2002), and therefore DOP is an important variable to be considered in the validation. The model reproduces values of DOP of the same order and higher than DIP values. Simulated values are almost in the range of the observed ones for all the areas (Tab. B3). A slight underestimation is shown for the northern sub-basin. The high variability of available data does not allow to appreciate the capability of the model results in reproducing the seasonal cycle and differences in the water column.

DOP mmol/m^3			MODEL		OBSERVATIONS		
Area	Depth	Time	Median	Min–max		Type of data	Reference
NA	Surf	Sum	0.07	0.04-0.16	0.05-0.1	min-max range	Ivancic et al.(2010a), sampling stations along Po-Rovinj section Fig. 4
	Surf	Aut	0.05	0.03-0.26	0.1-0.4	min-max range	Ivancic et al. (2010a), sampling stations along Po-Rovinj section, Fig. 4
NA, western	Surf	Aut-Win	0.08	0.04-0.26	0.3-0.4	min-max range	Ivancic et al. (2010b), sampling stations along Po-Rovinj section Fig. 3
	Bottom	Aut-Win	0.05	0.03-0.16	0.2-0.5	min-max range	Ivancic et al. (2010b), sampling stations along Po-Rovinj section Fig. 3
	Bottom	Sum	0.09	0.06-0.16	0.1-0.2	min-max range	Ivancic et al. (2010b), sampling stations along Po-Rovinj section Fig. 3

	Bottom	Sum	0.05	0.04-0.13	0.1-0.3	min-max range	Ivancic et al. (2010b), sampling stations along Po-Rovinj section Fig. 3
NA	Whole column	Win	0.08	0.05-0.14	0.085 (0.005-0.2)	mean and min-max	Cozzi et al. (2002), sampling Feb-Mar 1997
	Whole column	Annual	0.1	0.04-0.38	0.13	Mean	Lipizer et al. (1998), data of PRIMA project
CA	Surf	Annual	0.05	0.02-0.10	0.01-0.2	min-max range	Danovaro et al. (2005)

Tab. B3. Comparison between model and observation reported in literature for DOP (mmol/m^3).

B.5. Ecosystem processes

The range of variability of the primary production among the different areas of the Adriatic Sea is considerable (Tab. B4). The model reproduces the main observed spatial gradients: from the eutrophic western coastal strips to the off-shore areas, and from the NA to the CA and SA. Means and standard deviations of the model outputs are within the range of observed ones. It is worth noting that a perfect match between model and observation is not expected given that observations typically refer to limited areas and moments.

The observed range of the bacterial carbon production in coastal and off-shore areas of NA is well reproduced by the model (Tab. B4), confirming the capability of the model to reproduce some of the most relevant processes of the carbon cycle of this ecosystem.

Simulated sinking values are reported at the same depth of observations (by linearly interpolating the values at the nearest vertical model grid-points). The simulated sinking values of POC are in the range of the observed data in the different areas, except during the post bloom phase (March-June) in SA. The model, indeed, simulates an increment of sink for the post bloom phase (see Fig. 9 in the manuscript), but lower than that reported in the literature.

The table B4 shows a slight underestimation of the POC sinking at 1050 m in SA. This is likely due the organic matter remineralisation that occurs during the sinking phase, whereas in the model, that does not take into account refractory organic material dynamics, might overestimate the remineralization rate.

The simulated values of sinking at the central part of the CA is higher than that reported by Giordani et al. (2002), however, considering the sum of the reported values for burial and mineralization, the authors propose values of 15.7 g/m2/y (43mg/m2/d) for the organic carbon that has reached the bottom, which is consistent with the model values.

Primary Production mg/m^2/d	Model 2007 and 2008		Observations		
	mean±std	range	data	Type of data	Reference
NA, within WAC	366±137	102-755	356-575	Range annual values	Pugnetti et al. (2006)
			591.8	Mean 20-40m depth	Giordani et al. (2002)
			410.9	Mean 40m depth	
NA, offshore area	210±77	68-346	329	Mean	Zoppini et al. (1995)
			164-246	Range annual values	Pugnetti et al. (2006)
			172.6-284.9	Range	Degobbis et al. (1986) reported by Giordani et al. (2002)
CA, central pit	153±97	41-430	180±63	Mean and st.dev.	Giordani et al. (2002)
			164-246	Range	Pucher- Petkovic and Marasovic (1988) reported by Giordani et al. (2002)

CA, eastern part	141±92	38-423	175 (125-250)	Mean (interannual range)	Grbec et al. (2009) Fig. 3, data after 1998
SA, central pit	185±111	38-542	265±50	Mean and st.dev.	Giordani et al. (2002)
SA, within coastal strip	175±95	76-456	250	Average	Miserocchi et al. (1999)

Bacterial Carbon Production µg/l/h	Model 2007 and 2008		Observations		
	Median	IRQ	data	Type	Reference
NA, coastal area	0.40	0.11-0.67	0.5 (0.10-1.0) 1.15 (0.4-6.0)*	Median (range IQ) (*very coastal point)	Del Negro et al. (2008)
NA, offshore area	0.07	0.03-0.19	0.125 (0-0.8) <0.01 (0-0.4)	Median (range IQ)	Del Negro et al. (2008)

Sink of organic matter (POC) mgC/m^2/d	Model 2007 and 2008		Observations		
	Mean±std	IQR range	data	Type	Reference
SA, central Pit at 150m depth	18.9±5.7	15.5-21.6	9.7	mean of 1 and half year samplings	Boldrin et al. (2002)
SA, central pit at 150 depth (values for March-June)	25.2±3.1	22.5-27.3	~22-42	Range of values from Fig. 9	Boldrin et al. (2002)
SA, central pit at 1050 depth	5.1±0.5	4.6-5.4	6.99	mean of 1 and half year samplings	Boldrin et al. (2002)
SA, central pit at 1050 depth (values for March-June)	5.2±0.3	5.0-5.4	~9-20	Range of values from Fig. 9	Boldrin et al. (2002)
SA, central pit at the bottom	5.1±0.5	4.6-5.4	7.1	Mean values of moored trap (from Fig. 6)	Giordani et al. (2002)
CA, central part at 180m	33.5±11.3	26.8-42-2	9.3	Data from Hamilton et al. (1999)	Giordani et al. (2002)

Tab. B4. Values of primary production (mgC/m2/d), bacterial carbon production (µgC/l/h), and sink of organic matter (mg/m^2/d) for several area of the Adriatic sea.

B.6. Carbonate system variables

The simulated values of pCO2 in the Gulf of Trieste (Fig. B7) are in agreement with the data reported in Figure 2 of Turk et al. (2010), in terms of both values and annual trend. A slight overestimation is simulated for spring values, being the model values 50 µatm higher than those reported by Turk et al. (2010). Further, the model reproduces qualitatively the differences between the 2007 and 2008 trends, based on available observations. In particular the model simulates lower values in April-May 2008 than April-May 2007 and lower values in autumn 2008 than autumn 2007 as it is reported by Turk et al. (2010). The observed values of pCO2 in August 2008, much higher than during the previous year, is not adequately simulated by the model. However, Turk et al. (2010) report that the thermal component of pCO2 (Fig. 10f of Turk et al. 2010) are very similar for the two years. This suggests the possibility that important local biogeochemical processes for this very shallow area of the basin are not well reproduced by the model, due to its coarse spatial resolution, although it could account correctly for the thermal effect on the CO_2 solubility.
Table B5 reports the comparison of seasonal values of pCO2 for the central part of the SA. Modelled values are in good agreement with estimates proposed by d'Ortenzio et al., 2008.
Using the statistics of DIC and alkalinity reported by Luchetta et al., (2010) for a winter cruise in NA, it is possible to assess that the simulated values are in the range of variation of observations (Tab. B6), even if, a slight underestimation for both modelled alkalinity and DIC values can be noted. The effect of the underestimation of DIC and alkalinity partly compensate in the calculation

of pCO2. However, it is possible to assess and error of 20% in the comparison of pCO2 calculated using the mean simulated and observed values.
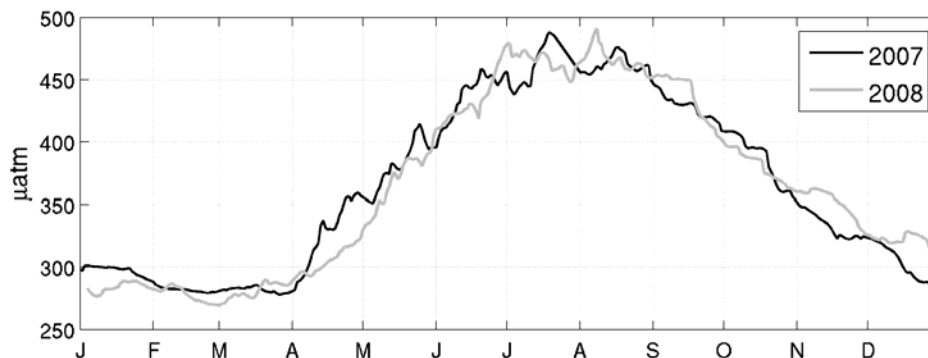
Fig B7. Trend of pCO2 in the Gulf of Trieste, to be compared with Figure 2 of Turk et al., 2010.

	Model Mean 2007-2008	Observations		
pCO2	Mean±std	data	Type	Reference
SA, surface central pit, winter	345±11	350	Value extracted from Fig.10.	D'Ortenzio et al., (2008)
SA, surface central pit, spring	411±44	400	Value extracted from Fig.10.	D'Ortenzio et al., (2008)
SA, surface central pit, summer	491±27	450	Value extracted from Fig.10.	D'Ortenzio et al., (2008)
SA, surface central pit, autumn	391±28	350-375	Value extracted from Fig.10.	D'Ortenzio et al., (2008)

Tab. B5. Values of pCO2 [µatm] in the central part of the Southern sub-basin.

	Model February 2008		Observations		
Alkalinity µmol/kg at 25°C	Mean±std	Min-max	data	Type	Reference
NA, surface off-shore area	2648±6	2636-2657	2658.9 ±18.1	Mean±st.dev of February 2008 (Tab. 3)	Luchetta et al. (2010)
DIC µmol/kg at 25°C					
NA, surface off-shore area	2335±15	2285-2371	2366.6 ±21.6	Mean±st.dev of February 2008 (Tab. 3)	Luchetta et al. (2010)

Tab. B6. Values of alkalinity and DIC for the off-shore northern sub-basin.

References:

Batistić M., Jasprica N., Carić M., Čalić M., Kovačević V., Garić R., Njire J.,Mikuš J., Bobanović-Ćolić S., 2011. Biological evidence of a winter convection event in the South Adriatic: A phytoplankton maximum in the aphotic zone, Cont. Shelf Res., doi:10.1016/j.csr.2011.01.004, 2011

Beck, J. R., and E. K. Shultz (1986), The use of relative operating characteristic (ROC) curves in test performance evaluation, Archives of Pathology and Laboratory Medicine, 110(1), 13–20.

Boldrin, A., Miserocchi, S., Rabitti, S., Turchetto, M. M., Balboni, V., and Socal, G.: Particulate matter in the Southern Adriatic and Ionian Sea: characterisation and downward fluxes, J. Marine Syst., 33–34, 389–410, 2002

Cloern, J.E., Grenz, C., Vidergar-Lucas, L.: An empirical model of the phytoplankton chlorophyll: carbon ratio-the conversion factor between productivity and growth rate, Limnol. Oceanogr., 40(7), 1313-1321, 1995

Cossarini, G., Solidoro, C., Fonda Umani, S.: Dynamics of biogeochemical properties in temperate coastal areas of freshwater influence: lessons from the Northern Adriatic Sea (Gulf of Trieste), Estuarine, Coastal and Shelf Science, 115, 63-74, 2012

Danovaro, R., Armeni, M., Luna, G.M., Corinaldesi, C., Dell'Anno, A., Ferrari, C.R., Fiordelmondo, C., Gambi, C., Gismondi, M., Manini, E.: Exo-enzymatic activities and dissolved organic pools in relation with mucilage development in the Northern Adriatic Sea, Science of the Total Environment, 353, 189-203, 2005

d'Ortenzio, F., Antoine, D., and Marullo, S.: Satellite-driven modeling of the upper ocean mixed layer and air-sea CO_2 flux in the Mediterranean Sea, Deep-Sea Res. Pt. I, 55, 405-434, 2008.

Fielding, A. H., Bell, J. F.: A review of methods for the assessment of prediction errors in conservation presence/absence models, Environmental Conservation, 24(01), 38–49, 1997

Giordani, P., Helder, W., Koning, E., Miserocchi, S., Danovaro, R., and Malaguti, A.: Gradient of benthis-pelagic coupling and carbon budgets in the Adriatic and Northern Ionian Sea, J. Marine Syst., 33–34, 365–387, 2002

Grbec, B., Morovic, M., Paklar, G.B., Kuspilic, G., Matijevic, S., Matic, F., Nincevic-Gladan, Z.: The relationship between the atmospheric variability and productivity in the Adriatic Sea area, Journal of the Marine Biological Association of the United Kingdom, doi:10.1017/S0025315409000708, 2009

Ivančić, I., Radic, T., Lyons, M.D., Fuks, D., Precali, R., Kraus, R.: Alkaline phosphatase activity in relation to nutrient status in the northern Adriatic Sea, Marine Ecology Progress Series, 378, 27-35, 2010a

Ivančić, I., Fuks, D. , Najdek, M., Blažina, M., Devescovi, M., Šilović, T., Paliaga, P., Orlić S.: Long-term changes in heterotrophic prokaryotes abundance and growth characteristics in the northern Adriatic Sea, Journal of Marine Systems, doi:10.1016/j.jmarsys.2010.05.008, 2010b

Karl, D.M., Björkman, K.M.: Dynamics of DOP, in: Biogeochemistry of Marine Dissolved Organic Matter, edited by Hansell, D.A., Carlson C.A., Academic Press, London, UK, 2002

Lipizer, M., Cozzi, S., Catalano, G.: Accumulation of DON and DOP and new production in the Northern Adriatic Sea, in: Dehairs, F.A. et al. (Ed.) . Integrated Marine System Analysis. European Network for Integrated Marine System Analysis FWO Vlaanderen: Proceedings of the second network meeting (Brussels, May 29-31, 1997). pp. 85-95, 1998

Luchetta, A., Cantoni, C., Catalano, G.: New observations of CO2-induced acidification in the northern Adriatic Sea over the last quarter century, Chemistry and Ecology, 26 (1), 1-17, 2010

Marini, M., Grilli, F., Guarnieri, A., Jones, B. H., Klajic, Z., Pinardi, N., and Sanxhaku, M.: Is the Southeastern Adriatic Sea coastal strip an eutrophic area?, Estuar. Coast. Shelf S., 88, 395–406., 2010

Miserocchi, S., Faganeli, J., Balboni, V., Heussner, S., Monaco, A., Kerheve, P.: Characteristics and sources of the settling organic matter in the south Adriatic basin, Organic Geochemistry, 30(6), 411-421, 1999

Querin, S., Cossarini, G., Solidoro, C.: Simulating the formation and fate of dense water in a mid-latitude marginal sea during normal and warm winter conditions, Submitted to JGS, 2012

Pucher-Petkovic, T., Marasovic, I.: Changes of productivity conditions in the open Middle Adriatic-eutrophication indicators, Pomor. Zb. 26, 585– 593,1988

Pugnetti, A., Camatti, E., Mangone, O., Morabito, G., Oggioni, A., Saggiomo, V.: Phytoplankton production in Italian freshwater and marine ecosystems: State of the art and perspective, Chemistry and Ecology, 22(1), S49-S69, 2006

Sheng, Y. P., Kim, T.: Skill assessment of an integrated modeling system for shallow coastal and estuarine ecosystems, Journal of Marine Systems, 76(1–2), 212–243, 2009

Solidoro, C., Bastianini, M., Bandelj, V., Codermatz, R., Cossarini, G., Canu, D.M., Ravagnan, E., Salon, S., Trevisani, S.: Current state, scales of variability, and trends of biogeochemical properties in the northern Adriatic Sea, Journal of Geophysical Research C: Oceans, 114(7), C07S91, doi:10.1029/2008JC004838, 2009

Turk, D., Malačič, V., DeGrandpre, M. D., and McGillis, W. R.: Carbon dioxide variability and air-sea fluxes in the Northern Adriatic Sea, J. Geophys. Res.-Oceans, 115, C10043, doi:10.1029/2009JC006034, 2010

Vilibic, I., Matijevic, S., Sepic, J.: Changes in the Adriatic oceanographic properties induced by the Eastern Mediterranean Transient, Biogeosciences Discuss., 9, 927–956, 2012

Volpe, G., Coltella, S., Forneris, V., Tronconi, C., Santoleri, R.: The Mediterranean Ocean Colour Observing System: system development and product validation, Ocean Sci. Discuss., 9, 1349–1385, 2012

Zavatarelli, M., Raicich, F., Bregant, D., Russo, A., Artegiani, A.: Climatological biogeochemical characteristics of the Adriatic Sea, J. Mar. Syst., 18, 227-263, 1998

Zoppini, A., Pettine, M., Totti, C., Puddu, A., Artegiani, A., Pagnotta, R.: Nutrients, Standing Crop and primary Production in Western Coastal Waters of the Adriatic Sea, Estuarine, Coastal and Shelf Science, 41, 493-513, 1995

Wiley, E. O., McNyset, K., Peterson, T., Robins, R., Stewart, A.: Niche modeling perspective on geographic range predictions in the marine environment using a machine-learning algorithm, Oceanography, 16(3), 120–127, doi:10.5670/oceanog.2003.42, 2003